Coherence and Intensity Statistical Mapping of Earthquake Affected Areas using Sentinel-1 Images

Rosalie Reyes [1,2], Masahiko Nagai [2]

[1] University of the Philippines, Department of Geodetic Engineering, Diliman, Quezon City, Philippines – rbreyes3@up.edu.ph
[2] Yamaguchi University, Center for Research and Application of Satellite Remote Sensing, Ube City, Yamaguchi, Japan - nagaim@yamaguchi-u.ac.jp

Keywords: Coherence, Intensity, earthquake affected areas, statistical mapping, Sentinel-1, threshold mapping

Abstract

The January 1, 2024, Noto Peninsula earthquake left many devastated areas. Right after the event, aerial photography provided the initial assessment but covered only specific areas. Satellite images with optical sensors that are freely available are limited by spatial resolution and oftentimes covered by cloud. The Sentinel-1 Synthetic Aperture Radar (SAR) due to its all-weather sensing capability proved to be useful in mapping the extent of the affected areas. This study mapped Wajima City where earthquake aftereffects were severe as reported using coherence and intensity mapping. Pre- and post-event images were used to rapidly identify affected areas. Based on the result, taking the coherence of one pre- and one post-event images can give an impression of wide earthquake damage. The coherence of two post-event images compared with two pre-event images provides a better estimate of affected areas. Taking multiple pre- and post- event images improved the map because the large variation of the intensity is minimized through time-series averaging. Using a simple RGB composite, the affected areas were mapped. Threshold mapping was also used to extract collapsed buildings/houses using a training dataset. The mean coherence difference and mean intensity difference between pre- and post-event images were the two variables used. The computed minimum threshold for the mean coherence difference was 0.35. However, the average not the minimum of the mean intensity difference of 3.0 was used as initial value. Using mean coherence difference>=0.35 gave a high accurate prediction of collapsed buildings at 73.47% but also has false identification of 30.95%. To negate the overprediction, the mean intensity difference<=4.0 was integrated. The result lowered the overprediction to 20.75% but also lowered the accuracy to 64.97%. This assessment was only conducted in the fire-razed morning market in Wajima City.

1. Introduction

Initial response upon news of a disaster is where it is located and how big is the area affected. Remote sensing, although with some limitations (e.g. spatial resolution), offers a bird’s eye view of the area and provides initial visual assessment. Basically, optical images provide the best information of the disaster affected area but oftentimes they are obscured by clouds and shadows. Radar remote sensing provides an all-weather observation data, albeit its salt and pepper appearance may prove challenging for some users. However, with advancement in technology and developed algorithms, it can go beyond visual analysis. Hence, inference of the images relies on other information that cannot be seen but serves as proxy for actual or ground observations. Disaster affected areas can be assessed remotely using derived information from said images.

The backscatter energy contains the information necessary for the interpretation of the targets being imaged and the basis for remote sensing with microwaves (Richards, 2009). This depends on the geometric and dielectric properties of the targets. The total power density of the incoming wave is its intensity (Ibid.). This is also defined as the wave amplitude squared (Zhou et al., 2009), an important consideration for analyzing the current state of the targets. Change in the properties of the object being imaged manifests in the variation of reflected intensity received by the radar sensor. However, the variation is also due to atmospheric influence (Ding, et al.,2008; Ferrettia et al., 2007). To minimize its effect, seasonality should be considered in the selection and analysis of the images. Coherence is another important parameter for detecting change derived from two Synthetic Aperture Radar (SAR) images. A detailed discussion on coherence estimation is given by Touzi et al., (1999). Waves that are in constant phase with each other are said to be coherent (Woodhouse, 2006). It is also the degree of correlation between the two constituent images of an interferometer that will take the value of 1 if fully correlated and 0 if fully decorrelated (Richards, 2009). Thus, a significant change in coherence means disturbance in the current state of the target from the previous. The formation of interferometric SAR images includes the coherence map output. Mapping using coherence and intensity estimation serves as preliminary assessment of damage caused by disaster.

The use of Sentinel-1 SAR images for mapping after disaster is becoming a popular choice due to its all-weather and side-looking imaging. Washaya et al., (2018) for example used Coherence Change-Detection (CCD) for monitoring natural and anthropogenic disasters in urban areas. Often mapping of damaged-affected areas after natural hazard events (Olen and Bookhagen, 2018; Donezar et al., 2019; Meneses and Blanco, 2022; Ge et al., 2019a) used coherence change because it can easily identify significant decorrelation. Several studies that are not only specific to utilizing Sentinel-1 but also other SAR sensors such as ALOS-2, TerraSAR-X etc. (Lu et al., 2018; Yun et al., 2015; Watanabe et al., 2012; Sharma et al., 2017) were conducted to map earthquake-induced damages utilizing coherence variation. Ge et al., (2019b) conducted building damage assessment using intensity from SAR data through change detection. This method is best when SAR satellites do not work in an interferometric mode (Ibid.).

Statistical mapping is another method for visually analyzing the change in an area that is abstracted, aggregated or simplified (Foster, 2019). This is because geospatial data is large and complex. The discretization of values in the field of statistics can be represented by histogram, interquartile range, standard deviation, outlier maps (Ibid.) and other representations derived from data calculations. Statistical maps can be from an analysis of a single image or many images. The latter is often referred to as multi-temporal or time series analysis. The resulting statistics derived from these maps indicate changes or no changes in areas of interest.

This contribution has been peer-reviewed. The double-blind peer-review was conducted on the basis of the full paper.
https://doi.org/10.5194/isprs-annals-X-3-2024-347-2024 | © Author(s) 2024. CC BY 4.0 License.

The mapping techniques discussed above were applied in this study to identify affected areas in Wajima City, Ishikawa Prefecture, Japan. The earthquake that occurred last January 1, 2024, with a magnitude of 7.5 caused damage particularly in these cities such as building collapse and landslides (The Yomiuri Shimbun, 2024a). In addition, the Geospatial Information (GSI) Authority of Japan mapped the emergence of land along the coast facing the Sea of Japan using the intensity change from ALOS-2 satellite (GSI, 2024a). This study focuses only on earthquake aftereffects in the urban areas. The aftereffects include building collapse, fire and tsunami damages. Coherence and intensity threshold based on the analysis of values from training dataset was also determined to facilitate the extraction of affected areas.

2. Materials and methods

2.1 Study areas

The study area is the city of Wajima (37.376 to 37.411 N; 136.833 to 136.917 E) located in the Noto Peninsula, Ishikawa Prefecture, Japan. This is one of the areas where earthquake aftereffects were severe as reported (The Japan Times, 2024). In Wajima City, close to 3800 houses collapsed (Crisis Management Office, 2024). Many houses were also consumed by the fire after the earthquake that razed Wajima Morning Market (NHK WORLD-JAPAN, 2024). Wajima City was selected to analyze the potential identification of affected areas using SAR coherence and intensity estimation with statistical mapping. Figure 1 shows the Noto Peninsula and the location of the study area.

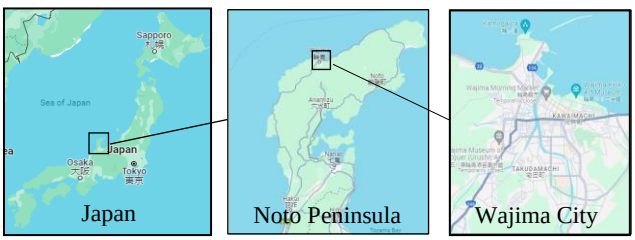

Figure 1. The study area (Google Map, n.d.).

2.2 Data and software used

There are 6 SLC images that were used for this study that were dated from 06 December 2023 to 02 February 2024. The Noto Peninsula earthquake happened on 1 January 2024 hence, there were 3 pre-event images and 3 post-event images acquired during the winter season. The decision to not only use one pre- and post- event images was to ensure the data consistency due to variations in the intensity. The VV polarization was selected for mapping the affected areas. The winter season images were chosen to avoid significant coherence variations due to season influence. The temporal variation was set at 12 days per image pair. The Copernicus 30m DEM (Digital elevation Model) was used for the terrain correction. The Google Earth images, photographs and aerial images from news agencies and GSI served as data for validation. Most of the Single Look Complex SAR images were downloaded from Alaska Satellite Facility (ASF) (n.d.) and Copernicus Browser (CB) (n.d.). The data used is listed in Table 1.

The Sentinels Application Platform or known as SNAP, was mostly used for processing the SAR images. This collection of toolboxes is being jointly developed by Brockmann Consult, CS France (FR), CS Romania (RO), SenSar (NL) and SkyWatch (CA) (eoPortal, n.d.). SNAP facilitates viewing, processing, and analyzing Sentinel products including remotely sensed data from other sensors. As it is a collection of free open-source toolboxes (Brochmann Consult GmbH, 2019), many users benefit from its many image processing functionalities. The SNAP latest version of SNAP is the SNAP 10.0.0 that can be downloaded from European Space Agency (ESA) Science Toolbox Exploitation Program (STEP) (ESA, n.d.).

SLC images	Provider
S1A_IW_SLC__1SDV_20231206	ASF
S1A_IW_SLC__1SDV_20231218	ASF
S1A_IW_SLC__1SDV_20231230	ASF
S1A_IW_SLC__1SDV_20240111	ASF
S1A_IW_SLC__1SDV_20240123	ASF
S1A_IW_SLC__1SDV_20240204	ASF
Copernicus 30m DEM	CB
Precise or restituted orbit files	CB

Table 1. Data used

2.3 Methods

The general workflow for determining earthquake affected areas is shown in Figure 2. The areas analyzed are concentrated in the urban areas where damaged to houses and buildings mostly occurred. The strong and weak backscatters from these targets prior to and after the earthquake respectively, provide information about what has changed. The method involves geometric and radiometric correction of the SLC images, coherence estimation of image pairs, subset to areas of interest (AOI), calculating statistics (mean and difference of coherence and intensity), and mapping damaged areas using RGB color composite, extraction of affected areas and validation using high resolution optical images.

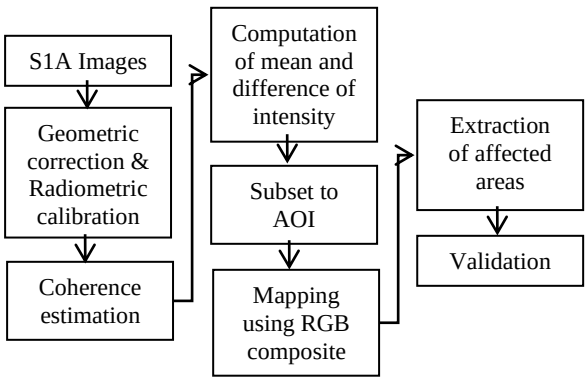

Figure 2. Workflow for mapping affected areas.

2.3.1 Processing

a) Geometric correction and radar calibration

The SLC images were geometrically corrected and radiometrically calibrated after downloading. Prior to these activities the required swath and bursts were selected using TOPSAR split. In this case the IW1 and bursts 2 and 5 were selected because these cover the area of interest. The Precise Orbit File (POEORB) or Restituted Orbit File (RESORB) (if POEORB is not available yet) that is automatically downloaded from Copernicus Browser was applied to provide accurate position of the SAR images. This ensures successful co-registration of several images. All individual images were radiometrically calibrated then debursted. The Multilook

function was applied to convert the pixel to square grid at the same time act as noise filter. Terrain Correction orthorectified the images using location and elevation information from the DEM.

b) Coherence estimation

Two successive SLC image files 12 days apart were processed for coherence estimation. For the initial damage assessment 3 SLC images were processed (2 pre-event images and 1 post-event image. In this case 2 coherence maps were produced. This is rapid mapping with the first SLC image acquired right after the event. With the availability of the second SLC image acquired after the event, 2 post-event images were processed together with the 2 pre-event images producing 3 coherence maps.

c) Computation of intensity mean and difference

Only the VV polarization was considered for mapping the earthquake aftereffects in the urban areas. The intensity of 2 successive images were averaged to produce the mean intensity map. Similarly, the difference between these images were taken to produce the difference of intensity map.

d) Subset to area of interest (AOI)

To speed up the processing, the urban areas where reports of damages occurred were cropped or clipped using the raster subset. Although, there are other areas in the Ishikawa Prefecture that were also affected but the city of Wajima has photos or aerial videos that can be used to validate the processing results.

e) Mapping RGB composite

The procedure for mapping using Red, Green and Blue (RGB) composite was adopted from tutorial by Chris Stewart (2017) of Earth Observation College. An additive RGB color composite display for initial visual assessment was used. The coherence was assigned in Red band, mean of intensity in Green band, and difference of intensity in Blue band. The combinations of the following produce: R + G = Yellow, G + B = Cyan and R + B = Magenta. For mapping urban areas for example where coherence is assigned to R and mean intensity is assigned to G the result is mostly yellow due to high coherence and high mean intensity.

f) Extraction of affected areas

For the initial extraction of the affected areas, coherence values >= 0.4, 0.5 and 0.6 were assumed. Using binary mapping with 1 as affected area and 0 as unaffected area the locations of affected areas were mapped.

g) Validation

The satellite images after the disaster were mostly cloudy, hence with shadows. Also, the limited spatial resolution posed difficulties in identifying affected areas. Fortunately, many news agencies captured many high-resolution images and aerial videos that could be used for the validation. The GSI of Japan immediately did aerial photography of the affected places right after the event. Once features from photographs were identified, these were located in Google Earth and the extent of affected areas digitized. Google Earth proved very helpful for providing pre-event high resolution images for validation.

2.3.2 Multi-temporal mapping of affected areas

The same procedure as discussed above was employed in mapping affected areas but in this case several images were considered. The SLC images used were selected within the winter season i.e. December to February. Taking the mean of intensity of several images can minimize the large variations in the intensity. Again, the images are grouped as pre-event and post-event images. This method can be used assuming that rebuilding of affected areas has not been completed. In addition to the method discussed, time series stacking of several images and determining threshold from values of randomly placed pins in the affected area were included (Figure 3). This time the variables for threshold mapping are 1) the difference of the mean of coherence between pre- and post- event maps and 2) the difference of the mean of intensity between pre- and post-event maps.

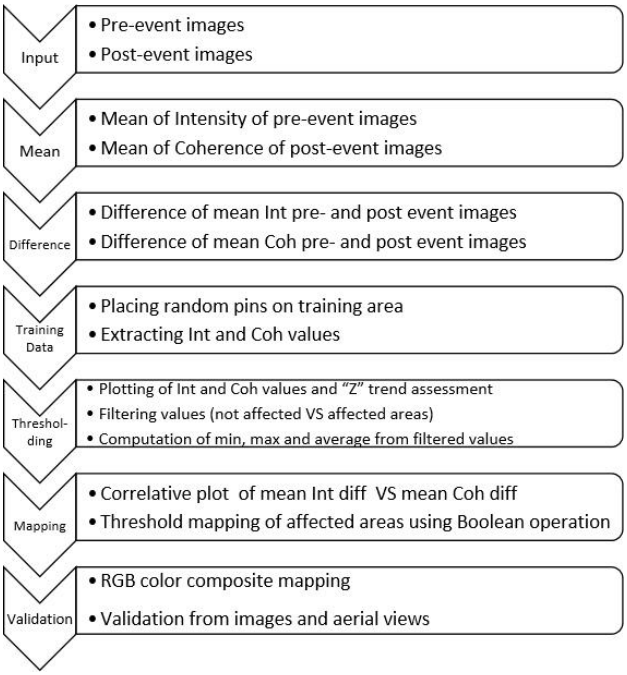

Figure 3. Multi-temporal mapping workflow.

3. Results and Discussions

3.1 Initial damage assessment

To initially visualize the areas that were affected right after the earthquake, 3 SLC images were used, and 2 coherence maps were produced. The RGB composite of pre-event map (18Dec23_30Dec23) in Figure 4a shows the dominance of the yellow pixels indicating high coherence and high mean of intensity. The pre- & post- event pair (30Dec23_11Jan24) are dominated by cyan and green colored pixels. This indicates low coherence as the yellow pixels are eclipsed (Figure 4b). There is a decrease of coherence throughout the area but said decrease does not necessarily indicate damaged areas. To produce the post-event map, 1 SLC image was added (23Jan23) as soon as it became available. Figure 4c is the post-event map (11Jan24_23Jan24) that shows the emergence of yellow pixels again. However, there are still areas where cyan and green pixels persist. Therefore, it is wise to consider additional image/s for confirmation.

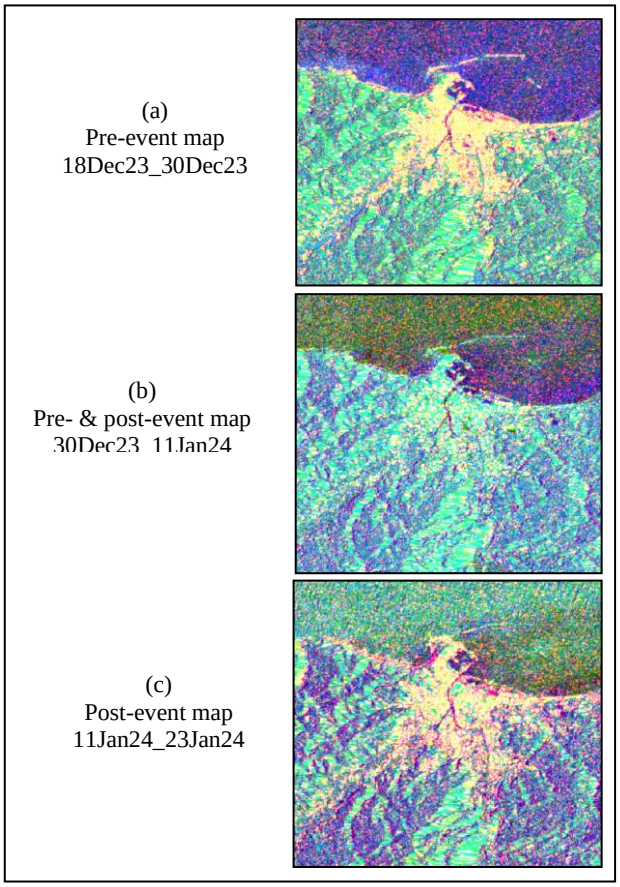

Figure 4. Comparison of pre-event; pre- & post- event; and post-event maps of affected areas (Yellow=high coh+high int; Cyan=high int+high int diff).

Taking the difference between coherence of image pairs can give a better indication of affected areas. The pre-event pair (18Dec23_30Dec23) coherence map was used as reference where pre- & post-event pair (30Dec23_11Jan24) and post-event (11Jan24_23Jan24) coherence maps were subtracted. The affected areas were extracted by assuming a coherence value >= 0.4, 0.5 and 0.6 using binary mapping. Of the 3 assumed values, coherence >=0.4 provides a better estimate. The results using coherence >= 0.4 are shown in Figure 5.

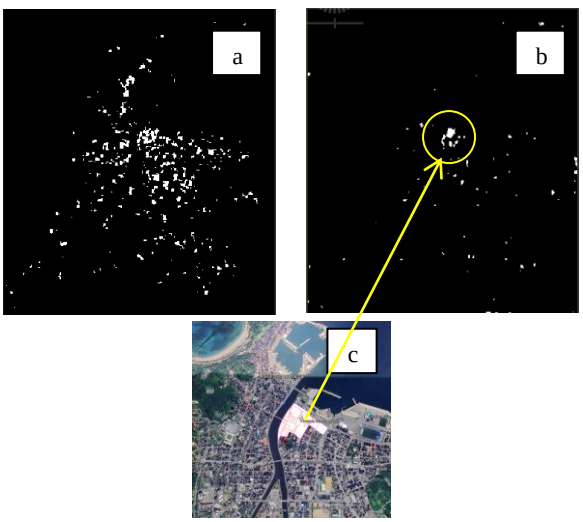

Figure 5. Difference of coherence (a) 18Dec23_30Dec23 minus 30Dec23_11Jan24; (b) 18Dec23_30Dec23 minus 11Jan24_23Jan 24; and (c) map of the affected area

The 18Dec23_30Dec23 minus 11Jan24_23Jan24 coherence maps better represents the affected areas. The actual affected area in Wajima City was delineated using high resolution aerial photography taken by GSI (2024b).

3.2 Multi-temporal mapping of affected areas

This method uses several images of SLC images. In this study a total of 6 images; 3 pre-event and 3 post-event images were processed. There are 5 coherence maps produced. The processed images and coherence maps were stacked into 2 groups: pre-event and post event time series maps. The mean of the intensity and coherence were computed for both time series. The differences of the means for the intensity and coherence were taken between pre- and post-event time series.

3.2.1 Threshold determination

Instead of assuming the threshold values for mapping, the thresholds for coherence and intensity are computed from training dataset composed of pixels in the known affected area. Pins were placed randomly in the said area and the values extracted. The map of the training area and the locations of the 50 pins is shown in Figure 6. This is the area where cyan and green pixels persist in the post-event map.

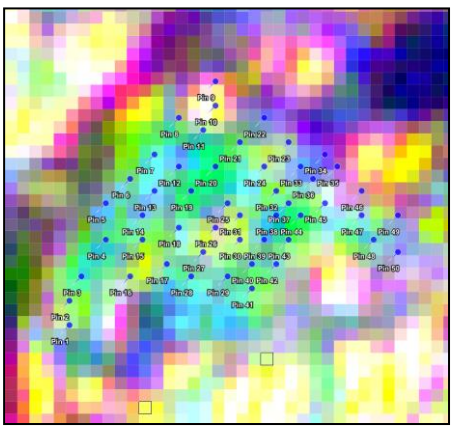

Figure 6. Locations of pins in the affected area.

The extracted values of the intensity were graphed to show the trend. The plots of the intensity in the affected and unaffected areas are shown in Figure 7.

The intensity in the affected areas (Figure 7a) showed a decrease after the event (11Jan24) but some increased on 23Jan24 but again decreased on 4Feb24. These variations in intensity pose a challenge for mapping affected areas especially in the urban areas where double bounces are prevalent. Out of 50 pins there were 28 pins that showed this trend. The rest of the pins showed a horizontal trend (Figure 7b). Although, it is expected that in the area known to be affected, the majority of the values will show a decrease after the event. This is assuming that many buildings have collapsed. However, backscatters from roads, parking areas and other open spaces may also contribute to this horizontal trend.

The trend of the coherence is shown in Figure 8. This is referred to here as the “Z” trend. A sudden decrease in coherence was also observed after the event but some increased in the 11Jan24_23Jan24 and 23Jan24_04Feb24 pairs.

This contribution has been peer-reviewed. The double-blind peer-review was conducted on the basis of the full paper.
https://doi.org/10.5194/isprs-annals-X-3-2024-347-2024 | © Author(s) 2024. CC BY 4.0 License.

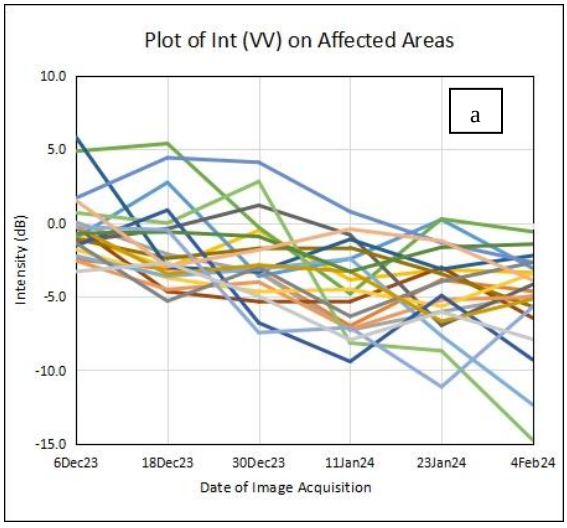

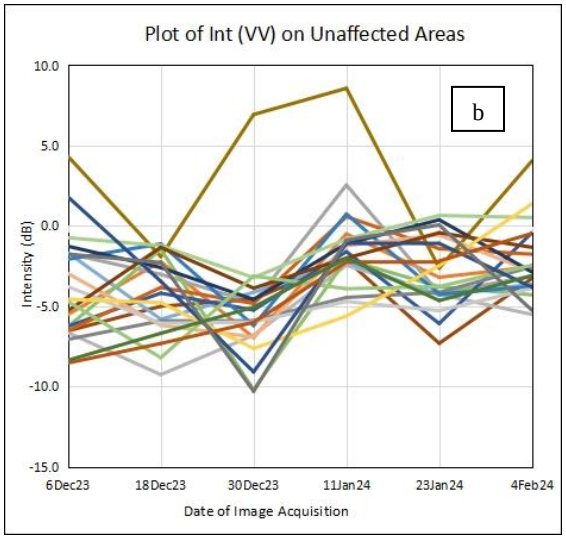

Figure 7. Trends of intensity in the (a) affected and (b) unaffected areas.

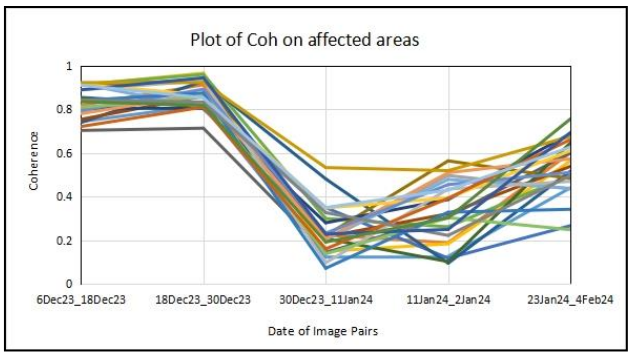

Figure 8. The “Z” trend of coherence.

A scatter plot between coherence and intensity was graphed to determine the correlation between the 2 variables. As shown in Figure 9, coherence has a negative correlation with intensity but is very low. This is due to the large variations in the intensity. Hence, using the mean of the intensity as threshold is better for mapping affected areas.

The threshold for the intensity was computed by taking the difference between the means of intensity in the pre-event and post event time series. A positive difference indicates affected areas. The min, max and average for the mean intensity difference were 0.13, 11.68 and 2.56 dB, respectively. Thus, threshold for intensity is the mean value that could take an initial value of 3.0.

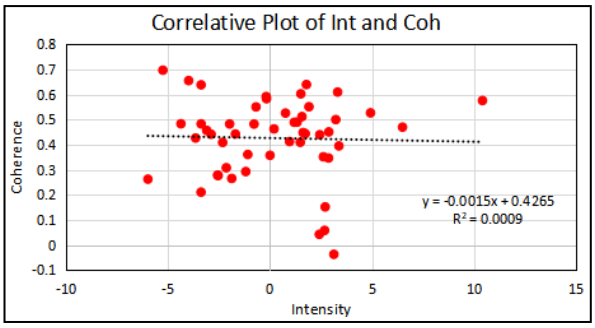

Figure 9. Correlative plot of coherence and intensity.

The same procedure was used for determining the threshold for coherence. The mean coherence difference between pre- and post-event time series has a min, max and average of 0.35, 0.64 and 0.49. The threshold for coherence can have a minimum value of 0.35.

3.3 Threshold mapping of affected areas

Using the computed minimum threshold for mean coherence difference, the affected areas are extracted. For comparison a value of 0.40 was also tested. The resulting maps for values of 0.35 and 0.40 are shown in Figure 10a and 10b, respectively. The top maps show the whole study area while the bottom maps are the zoomed-in views of the reported morning market in Wajima City that was razed by fire on January 1, 2024, after the earthquake. The polygons are the digitized areas of collapsed buildings.

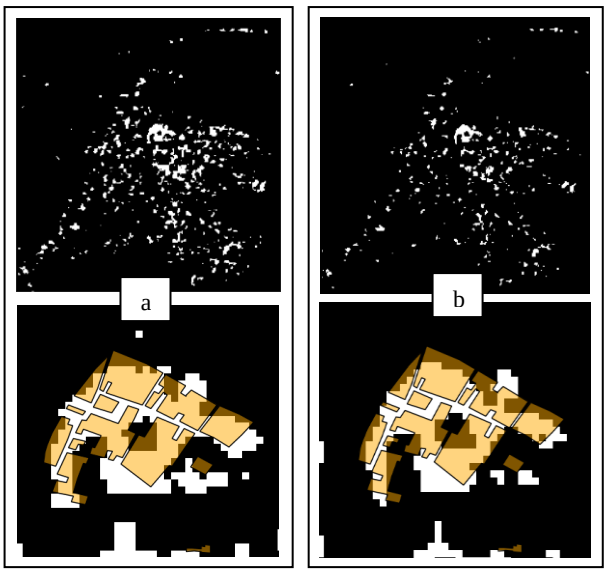

Figure 10. Maps of affected areas using mean coherence difference values of (a) >= 0.35 and >=0.40.

The maps extracted using mean coherence difference still includes unaffected areas. Combining the mean intensity difference with mean coherence difference was tested using Boolean operation. The mean intensity difference values of 3.0 and 4.0 were mapped for comparison. The results showed that a threshold value of 4.0 was less noisy. Thus, said value was used to combine with mean coherence difference values. Two

combinations were experimented: 1) mean coherence difference >=0.35 and mean intensity difference <= 4.0; and 2) mean coherence difference >=0.40 and mean intensity difference <= 4.0. Since the 2 variables are inversely proportional so the <= was used for the mean intensity difference. In this case the latter served as filter. The resulting maps are shown in Figure 11.

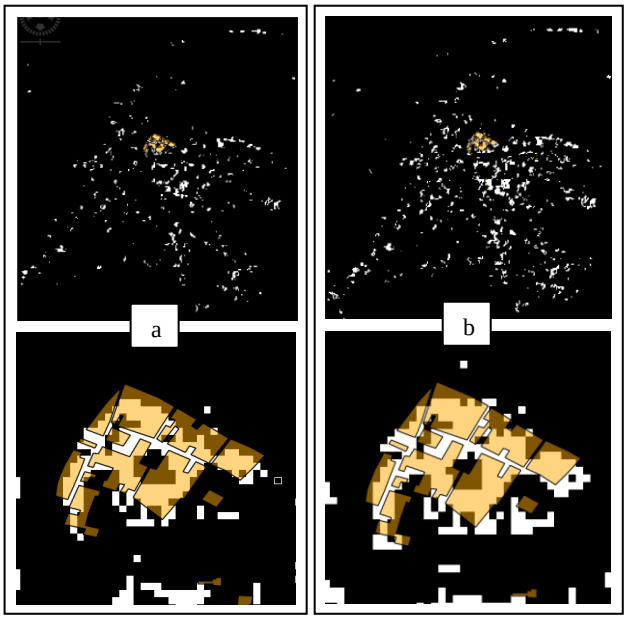

Figure 11. Maps of affected areas using combination of (a) mean coherence difference >=0.40 and mean intensity difference <= 4.0; and (b) mean coherence difference >=0.35 and mean intensity difference <= 4.0.

The maps in Figure 11 are less noisy than the maps extracted using mean coherence difference only (Figure 10). Some areas that were classified as affected areas wrongly were negated by integrating the mean intensity difference. However, during close inspection, there were open areas such as parking spaces and football/baseball fields that were mapped as affected. Isolated cases of buildings/houses collapsed were not mapped wherever they are surrounded by standing buildings. As reported, most of these collapsed houses were already old, thus the type of construction materials affects the strength of the backscatter. The resolution of the image at around 13m also contributed to some misclassifications. Usually, scatterers such as plain concrete and galvanized iron sheet roofing will dominate the backscatter in a mixed type of buildings/houses in urban setting.

The study area was also mapped using RGB composite using the mean of coherence, mean of intensity of the post-event images and the difference in the mean of intensity of pre- and post-event images from time-series stacking. The color composite map is shown in Figure 12 with the map taken from the The Yomiuri Shimbun (2024) based on the received data from aerial photographs taken by Kokusai Kogyo Co., for validation.

High resolution optical images, e.g. aerial photography, can effectively show areas of devastation from natural disasters but has limited area of coverage. Satellite images that have high spatial resolution can also be used but usually, they are not available freely. While Sentinel data are readily available at no cost they are also limited by spatial resolution. However, for indication of disaster affected area, these satellite images can already provide general information of the extent of the disaster.

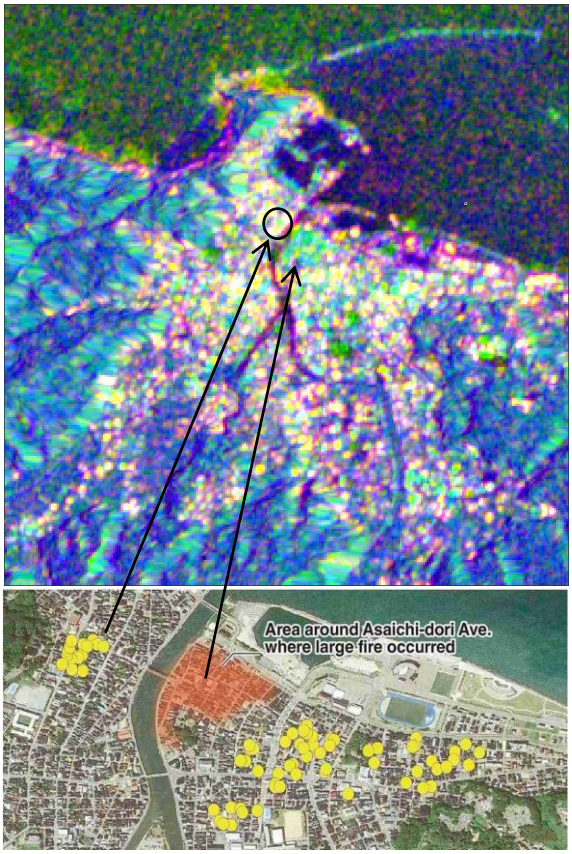

Figure 12. (Top) RGB composite map of affected areas from time-series averaging of coherence and intensity and (bottom) map of destroyed buildings in Wajima City (The Yomiuri Shimbun, 2024b).

3.4 Accuracy assessment

The accuracy assessment was made only on fire-razed morning market in Wajima City. The digitized polygons covering the collapsed/devastated buildings were used as ground truth. The conditions set as discussed above were the best representation of the affected areas. Table 2 is the summary of the accuracy assessment.

Conditions	Accurately predicted	Under predicted	Over predicted
A. Mean coh diff≥0.35	73.47	26.53	30.95
B. Mean coh diff≥0.40	62.93	37.07	21.77
C. Mean coh diff≥0.35 and Mean int diff≤4.0	64.97	35.03	20.75
D. Mean coh diff≥0.40 and Mean int diff≤4.0	57.14	42.86	11.22

Table 2. Accuracy assessment (%)

Although condition A has the highest percentage of pixels accurately predicted and the lowest underpredicted or unidentified pixels, it has also the highest overpredicted pixels or pixels falsely identified as collapsed buildings. Condition C negated the overprediction of Condition A, but it has resulted in lowering the accuracy and increasing the missed pixels but

This contribution has been peer-reviewed. The double-blind peer-review was conducted on the basis of the full paper.
https://doi.org/10.5194/isprs-annals-X-3-2024-347-2024 | © Author(s) 2024. CC BY 4.0 License.

performed better than Conditions B and D. Further studies could improve the results by incorporating other conditions or improving the process.

4. Conclusions

A combination of coherence and intensity images can be used to identify in general areas affected by earthquake right after disaster using RGB color composite. However, the method presented cannot identify specific locations of isolated collapsed buildings/houses due to the limitation of the spatial resolution and large variations in the intensity caused by signal double bounces in the urban area. The type of roofing materials such as ceramic tiles, plain concrete and galvanized iron sheet also contribute to the variations. In the case of the study area where old houses are mixed with new buildings, the intensity within a pixel is dominated by strong scatterers. Thus, there are collapsed houses not mapped because the surrounding buildings are giving a strong backscatter.

A minimum threshold of 0.35 from mean coherence difference between pre- and post-event maps derived from time series images can be used to extract affected area but this may vary depending on the area. Due to the large variations in the intensity, the mean or average of the intensity was used instead of the minimum. Threshold mapping using mean coherence difference>=0.35 gave the highest accuracy of identifying collapsed buildings at 73.47% but also has the highest false identification at 30.95%. To negate the overprediction the condition of mean intensity difference<=4.0 was added. This lowered the overprediction to 20.75% but as a consequence reduced the accuracy to 64.97%.

References

Alaska Satellite Facility, n.d.: https://search.asf.alaska.edu/#

Brochmann Consult GmbH, 2019: Sentinels Application Platform (SNAP). https://www.brockmann-consult.de/portfolio/earth-scientific-image-processing/

Copernicus Browser, n.d.: https://browser.dataspace.copernicus.eu/

Crisis Management Office, 2024: Regarding the status of damage caused by the 2024 Noto Peninsula Earthquake as of March 19, 2024. Retrieved March 21, 2024. https://www.pref.ishikawa.lg.jp/saigai/documents/higaihou_111_0319_1400.pdf.

Ding, X., Li, Z., Zhu, J., Feng, G., Long, J., 2008: *Sensors 2008, 8, 5426-5448*; doi: 10.3390/s8095426.

Donezar, U., De Blas, T., Larrañag, A., Ros, F., Albizua, L., Steel, A., Broglia, M. 2019: Applicability of the MultiTemporal CoherenceApproach to Sentinel-1 for the Detection and Delineation of Burnt Areas in the Context of the Copernicus Emergency Management Service. *Remote Sens. 2019, 11, 2607*. doi:10.3390/rs11222607.

eoPortal, n.d.: https://www.eoportal.org/other-space-activities/snap-sentinel-application-platform#snap-sentinel-application-platform-toolbox

ESA, n.d.: Science Toolbox Exploitation Platform (STEP). https://step.esa.int/main/download/snap-download/

Ferretti, A., Monti-Guarnieri, A., Prati, C., Rocca, F., 2007: *InSAR Principles: Guidelines for SAR Interferometry Processing and Interpretation*. ESA Publication, ESTEC, Noorwijk, The Netherlands.

Foster, M., 2019: Statistical Mapping (Enumeration, Normalization, Classification). *The Geographic Information Science & Technology Body of Knowledge (2nd Quarter 2019 Edition), John P. Wilson (Ed.)*. doi: 10.22224/gistbok/2019.2.2.

Ge, P., Gokon, H., Meguro, K., Koshimura, S., 2019a: Study on the Intensity and Coherence Information of High-Resolution ALOS-2 SAR Images for Rapid Massive Landslide Mapping at a Pixel Level. *Remote Sens. 2019, 11(23), 2808.* https://doi.org/10.3390/rs1123280.

Ge, P., Gokon, H., Meguro, K., 2019b: Building Damage Assessment Using Intensity SAR Data with Different Incidence Angles and Longtime Interval. *Journal of Disaster Research Vol.14 No.3, 2019*. https://doi.org/10.20965/jdr.2019.p0456.

Google Map, n.d.: Noto Peninsula, Japan. Available at: https://www.google.com/maps/@37.1627055,137.031381,10.25z?entry=ttu.

GSI, 2024a: Coastline change caused by the 2024 Noto Peninsula Earthquake detected by ALOS-2 SAR satellite image (Jan. 4, 2024). https://www.gsi.go.jp/uchusokuchi/uchusokuchi-e31001.html.

GSI, 2024b: Information regarding the 2024 Noto Peninsula Earthquake. Published on January 4th, 2024. https://www.gsi.go.jp/BOUSAI/20240101_noto_earthquake.html#1-2.

Lu, C., Ni, C., Chang, C., Yen, J., Chuang, R., 2018: Coherence Difference Analysis of Sentinel-1 SAR Interferogram to Identify Earthquake-Induced Disasters in Urban Areas. *Remote Sens. 2018, 10, 1318*. doi:10.3390/rs10081318.

Meneses, S., Blanco, A., 2022: Rapid Mapping and Assessment of Damages Due to Typhoon Rai Using Sentinel-1 Synthetic Aperture Radar Data. *The International Archives of the Photogrammetry, Remote Sensing and Spatial Information Sciences, Volume XLIII-B3-2022, XXIV ISPRS Congress (2022 edition), 6–11 June 2022, Nice, France.*

NHK WORLD-JAPAN, 2024: Fire burns down Wajima’s Asaichi Street. https://www3.nhk.or.jp/nhkworld/en/news/ataglance/2893/

Olen, S., Bookhagen, B., 2018: Mapping Damage-Affected Areas after Natural Hazard Events Using Sentinel-1 Coherence Time Series. *Remote Sens. 2018, 10, 1272.* doi:10.3390/rs10081272.

Richards, J. A., 2009: *Remote Sensing with Imaging Radar*. Springer.

Sharma, C.R., Tateishi, R., Hara, K., Nguyen, T.H., Gharechelou, S., Nguyen, V.L.: Earthquake Damage Visualization (EDV) Technique for the Rapid Detection of Earthquake-Induced Damages Using SAR Data. *Sensors 2017, 17, 235.*

Stewart, C., 2017: ESA Echoes from Space - Land Urban Footprint Mapping with Sentinel-1. EO College. https://www.youtube.com/watch?v=JslESstEIVw

The Japan Times, 2024: Japan quake death toll tops 200 as police comb burned-down market. https://www.japantimes.co.jp/news/2024/01/09/japan/ishikawa-earthquake-wajima-search/

The Yumiuri Shimbun, 2024a: Noto Peninsula Earthquake damage situation map. https://japannews.yomiuri.co.jp/society/noto-peninsula-earthquake/20240114-162072/.

The Yumiuri Shimbun, 2024b. “Over 1,300 House Destroyed or Damaged in Noto Earthquake; Situation in Hard-Hit Cities Still Difficult to Ascertain”, January 8, 2024. Accessed February 20, 2024. https://japannews.yomiuri.co.jp/society/noto-peninsula-earthquake/20240108-160699/

Touzi, R., Lope, A., Bruniquel, J., Vachon, P. W., Coherence Estimation for Sar Imagery. *IEEE Transactions on Geoscience and Remote Sensing (Volume: 37, Issue: 1, January 1999).* doi: 10.1109/36.739146.

Washaya, P., Balz, T., Mohamadi, B., 2018: Coherence Change-Detection with Sentinel-1 for Natural and Anthropogenic Disaster Monitoring in Urban Areas. *Remote Sens. 2018, 10, 1026.* doi:10.3390/rs10071026.

Watanabe, M, Motohka, T., Miyagi, Y., Yonezawa, C., Shimada, M., 2012: Analysis of Urban Areas Affected by the 2011 Off the Pacific Coast of Tohoku Earthquake and Tsunami With L-Band SAR Full-Polarimetric Mode. *IEEE Geosci. Remote Sens. Lett. 2012, 9, 472–476.*

Woodhouse, I., 2006: *Introduction to Microwave Remote Sensing*. CRC Press, Boca Raton, FL, USA. https://doi.org/10.1201/9781315272573.

Yun, S., Hudnut, K., Owen, S., Webb, F., Simons, M., Sacco, P., Gurrola, E., Manipon, G., Liang, C., Fielding, E., et al., 2015: Rapid Damage Mapping for the 2015 Mw 7.8 Gorkha Earthquake Using Synthetic Aperture Radar Data from COSMO–SkyMed and ALOS-2 Satellites. *Seismol. Res. Lett. 2015, 86, 1549–1556*.

Zhou, X., Chang, N., Li, S., 2009: Applications of SAR Interferometry in Earth and Environmental Science Research. *Sensors 2009, 9, 1876-1912.* doi:10.3390/s90301876.